On the Instantaneous Phase and Frequency Estimation of a Non-stationary Signal. The JADE Algorithm

Jayanth C. Mouli* , *Student Member, IEEE,* David V. Anderson* *Senior Member, IEEE*, Antonio Cicone†‡§
*School of Electrical and Computer Engineering, Georgia Institute of Technology, Atlanta, GA, USA {jmouli, anderson}@gatech.edu †DISIM, University of L'Aquila, L'Aquila, Italy. antonio.cicone@univaq.it ‡Institute of Astrophysics and Spatial Planetology of the National Institute of Astrophysics, Rome, Italy. § National Institute of Geophysics and Vulcanology, Rome, Italy.

***Abstract*—Many real-life signals such as gravitational wave measurements, biomedical signals, or geophysical data are strongly non-stationary but can be decomposed into mono-component signals that contain only one active frequency over time. The problem is how to compute, in an accurate and stable way, the instantaneous frequency, phase, and amplitude of such mono-component signals. Numerous approaches have been developed so far, but they are unstable in the presence of noise, and have a hard time capturing quick instantaneous changes in frequency. In this work, we present an alternative approach, called the JADE method, which is based on the Dynamic Time Warping algorithm. We test its robustness to noise and run comparisons with classical methods used for instantaneous frequency, phase, and amplitude.**

***Index Terms*—Instantaneous Frequency, Instantaneous Phase, Non-stationary Signal, AM/FM Demodulation**

I. Introduction

REAL-life signals are non-stationary in general. They are generated by complex and nonlinear systems. In recent years many innovative algorithms have been developed that are able to decompose real-life signals into simple oscillatory components. We can think, for instance, of Empirical Mode Decomposition [1], Iterative Filtering [2], [3], Ensemble empirical mode decomposition [4], sparse time-frequency representation [5], Geometric Mode Decomposition [6], Variational Mode Decomposition [7], Empirical wavelet transform [8], and Resampled Iterative Filtering [9], just to mention a few.

Once a signal has been decomposed into simple oscillatory and non-stationary components, there is a need to study their frequency content to characterize them. Many papers have been published in the past introducing the concept of instantaneous frequency and reviewing the methods developed for its computation [10]–[20].

Among the approaches developed so far, we recall here the estimation of the instantaneous frequency of a signal based on the time-frequency representations [12], [21], and its variant which is based on nonparametric estimation based on the maxima position of the time-frequency representation [10], [11]. Other approaches are based on the intersection of the confidence intervals [22] and the modified intersection of the confidence intervals [23] algorithms, Wigner-Ville distribution [24], cross Wigner-Ville distribution [25], directionally smoothed polynomial Wigner–Ville distribution [26], [27], robust Wigner distribution [28], spectrogram with varying window length [29], Hilbert Transform [1] and Normalized Hilbert Transform [16], peeling, i.e. the maxima position of the strongest component [30], the generalized zero-crossing (GZC) [16], segmentation processes based on mathematical morphology [31], [32], Synchrosqueezing transform [17], IM-Fogram [33], [34], and many more [20].

Even though many different methods have been proposed in the literature, they can be unstable to noise and, more importantly, cannot capture intrawave modulations in the frequency, i.e. variation that takes place even inside each period of the oscillatory components. All these methods are designed to capture up to interwave modulations in frequency, i.e. changes in frequency that take place from one period to the next one. However, non-stationary signals are, in general, intrawave modulated [16]. As an example, we can consider, for instance, a biomedical signal like the electrocardiogram of a patient [35], or an astrophysical signal like a gravitational wave produced by the collision of two black holes in deep space [36], or a geophysical signal as the Earth's magnetic field measured through a satellite orbiting around the globe [37]. All these signals present rapid changes in their frequency content. To be properly analyzed they require an algorithm able to capture the instantaneous frequency contained in them. In this work, we propose an innovative approach that is based on the so-called Dynamic Time Warping algorithm, and we show its robustness against noise compared to traditional methods available in the literature.

The rest of this work is organized as follows: in Section II we review a few methods for the computation of the instantaneous frequency of a monocomponent signal and then we propose our approach. In Section III results relative to a few artificial examples are presented, including the test of the robustness of the proposed method and previously published techniques to noise. Section IV concerns the application of the proposed method to a few real-life applications. In the last section, we derive conclusions and highlight future directions of research.

II. Methods

A. Instantaneous Frequency Estimation Methods

Non-stationary signals are characterized by their instantaneous frequency (IF), which is defined as the local frequency of the signal at a specific time. We describe several methods to compute the IF of a monocomponent signal in this section. IF is commonly computed through the analytic signal produced by the Hilbert transform (HT). For an input signal $x(t)$, this approach constructs the complex-valued analytic signal $Z(t) = x(t) + j\hat{x}(t)$, where

$$\hat{x}(t) = \frac{1}{\pi} P.V. \int_{-\infty}^{+\infty} \frac{x(\tau)}{t-\tau} d\tau \tag{1}$$

is the Hilbert Transform of $x(t)$, and the phase $\phi(t)$ is the angle of $Z(t)$ [1]. The IF of the signal, $\omega(t)$, is then obtained from:

$$\omega(t) = \frac{1}{2\pi} \frac{\mathrm{d}\phi(t)}{\mathrm{d}t} \tag{2}$$

Huang et al. [16] determined that several conditions, including those proposed by Bedrosian [38] and Nuttall [39], need to be satisfied to obtain an accurate IF estimate using the HT analytic signal approach. To satisfy these conditions, Huang et al. [16] introduced the Normalized Hilbert Transform (NHT) approach, in which an empirical method separates amplitude modulation (AM) from frequency modulation (FM). In this method, a cubic spline curve $e_1(t)$ is fit to the envelope of the signal, and this curve is used to normalize the input $x(t)$:

$$y_1(t) = \frac{x(t)}{e_1(t)}, \tag{3}$$

where $y_1(t)$ is the normalized signal. This normalization scheme is applied iteratively until all signal values are less than or equal to unity. After the nth iteration, the normalized signal

$$y_n(t) = \frac{y_{n-1}(t)}{e_n(t)}, \tag{4}$$

is only frequency modulated, with the AM component removed. The IF of the normalized signal $y_n(t)$ is then computed using the HT analytic signal approach.

Another IF estimation method proposed by Huang et al. [16] is Direct Quadrature (DQ), which also uses the previously described normalization scheme. Here, assuming the original signal $x(t) = A(t)y_n(t)$, and $y_n(t) = cos(\phi(t))$, the quadrature of $y_n(t)$ is computed as $\sqrt{1 - y_n(t)^2}$. The phase is obtained as:

$$\phi(t) = \arctan \frac{y_n(t)}{\sqrt{1 - y_n(t)^2}} \tag{5}$$

The IF is then computed from the derivative of Eq. 5. The advantage of the DQ approach is that it bypasses the HT integral and solely computes the phase from differentiation.

B. Dynamic Time Warping

Dynamic Time Warping (DTW) is a widely used algorithm to compare time series data by performing a temporal alignment. DTW is capable of determining the optimal alignment despite differing lengths and time shifts of input signals. Suppose there are two time series $\mathbf{X} = [x_1, ..., x_n]$ and $\mathbf{Y} = [y_1, ..., y_m]$ of lengths n and m respectively. The two series can be aligned to form a cost matrix $\mathbf{D} \in \mathbb{R}^{n \times m}$. The cost matrix $\mathbf{D}$ is initialized under two constraints:

- $\mathbf{D}_{i,0} = \infty$ for $i \in [1, n)$ and $\mathbf{D}_{0,j} = \infty$ for $j \in [1, m)$
- $\mathbf{D}_{0,0} = 0$

The local distance measure $d(\cdot, \cdot)$ used in this study is the Euclidean distance. The matrix $\mathbf{D}$ is then populated according to the formula:

$$\mathbf{D}_{i,j} = d(\mathbf{X}_i, \mathbf{Y}_j) + \min \begin{Bmatrix} \mathbf{D}_{i-1,j-1} \\ \mathbf{D}_{i-1,j} \\ \mathbf{D}_{i,j-1} \end{Bmatrix} \tag{6}$$

A warping path $\mathbf{P}$ is a set containing the indices of the aligned elements: $\mathbf{P} = [(i_1, j_1), ..., (i_L, j_L)]$. $\mathbf{P}$ is defined as a path through the cost matrix $\mathbf{D}$ that satisfies the following conditions:

- $\mathbf{P}_1 = (i_0, j_0) = (0, 0)$
- $\mathbf{P}_L = (i_L, j_L) = (n-1, m-1)$
- $i_{k-1} \leq i_k \leq (i_{k-1} + 1)$ for $k \in (1, L)$
- $j_{k-1} \leq j_k \leq (j_{k-1} + 1)$ for $k \in (1, L)$

The cost C_P of a given path $\mathbf{P} = [(i_1, j_1), ..., (i_L, j_L)]$ is defined as:

$$C_P = \sum_{k=1}^{L} \mathbf{D}_{i_k, j_k} \tag{7}$$

With the set of all possible paths $\mathbf{P}$ defined as $\mathbb{P}_{n,m}$, the optimal path $\mathbf{\Omega}$ is:

$$\mathbf{\Omega} = \arg\min_{\mathbf{P}} \{C_P | \mathbf{P} \in \mathbb{P}_{n,m}\} \tag{8}$$

This path $\mathbf{\Omega}$ can be determined by tracing back through the cost matrix from $\mathbf{D}_{n-1,m-1}$ to $\mathbf{D}_{0,0}$. The cost $C_{\mathbf{\Omega}} = DTW(\mathbf{X}, \mathbf{Y})$ of $\mathbf{\Omega}$ is often used as a metric of similarity between the inputs $\mathbf{X}$ and $\mathbf{Y}$.

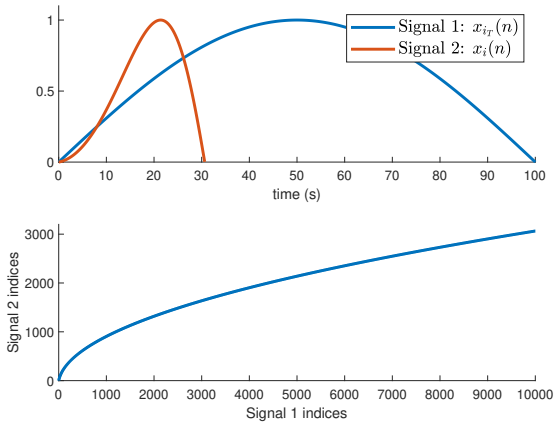

Fig. 1. Example of DTW alignment between two signals. The original signals (top) are aligned according to the warping path (bottom).

C. JADE algorithm

In this study, we use DTW as a tool to estimate the instantaneous phase and frequency of an input signal. We call this newly developed approach the JADE algorithm, from the initials of the author's names and the word estimator. Consider a sampled signal $x(n) = cos(\phi(n))$, where T_s is the sampling period. Assume $x(n)$ is time-warped using DTW to align with a discrete-time template signal $x_T(k) = cos(\omega_T k T_s)$, where ω_T is the known template frequency. $x(n)$ can be expressed as $cos(\omega_T \psi(n))$ where $\psi(n) = \frac{\phi(n)}{\omega_T}$. After the DTW alignment, the optimal warping path $\mathbf{\Omega}(k)$ approximates the following relation:

$$x(\mathbf{\Omega}(k)) = cos(\omega_T \psi(\mathbf{\Omega}(k))) \approx cos(\omega_T k T_s) \tag{9}$$

Therefore, $\psi(\mathbf{\Omega}(k)) = T_s k$, and:

$$\mathbf{\Omega}^{-1}(k) = \frac{1}{T_s}\psi(k) = \frac{1}{\omega_T T_s}\phi(k) \tag{10}$$

By time-warping $x(n)$ into a known template signal using DTW, the phase $\phi(n)$ can be recovered using the warping path $\mathbf{\Omega}(k)$. This study leverages the relationship in (10) to estimate the phase of input signals. Then, by applying (2) we compute the corresponding instantaneous frequency.

The discrete-time signal model we use to represent a zero-mean oscillatory signal $x(n)$ is $x(n) = cos(\phi(n)) + w(n)$, where $w(n)$ is Gaussian noise, and the function $\phi(n)$ is to be estimated. The noise can cause several problems with finding $\phi(n)$. First, we have found that when $x(n)$ is non-monotonic, the noise can have an impact on $\phi(n)$ in particular around the inflection point. Accordingly, we may elect to break the signal into monotonic segments for further analysis. Alternatively, we can break the signal into segments at the zero crossings. We denote the k zero-crossings of $x(n)$ as $\mathbf{z} = \{z_1, ..., z_k\}$. Because the noise $w(n)$ can interfere with zero-crossing detection, a smoothed version of $x(n)$, $x_s(n)$, is created by applying a moving average window with a fixed window length. A heuristic estimates the window length that attenuates 25% of the energy of the signal $x(n)$. The zero-crossings $\mathbf{z}$ are then determined:

- $i \in \mathbf{z}$ if $x_s(i-1) < 0 < x_s(i), i \in n$
- $i \in \mathbf{z}$ if $x_s(i) < 0 < x_s(i-1), i \in n$

Next, $x(n)$ is split into sections $\mathbf{x}_k = \{x_1(n), ..., x_k(n)\}$ at zero-crossing indices $\mathbf{z} = \{z_1, ..., z_k\}$. Each section $x_i(n) \in \mathbf{x}_k$ is defined by:

$$x_i(n) = \begin{cases} x(n + z_i) & \text{if } 0 \le n \le (z_{i+1} - z_i) \\ 0 & \text{if } n > (z_{i+1} - z_i) \end{cases} \tag{11}$$

Each section $x_i(n) \in \mathbf{x}_k$ resembles a half-period sinusoid, which we denote the template sinusoid $x_{i_T}(n)$. The template sinusoid has amplitude A_{i_T} and frequency ω_{i_T}. The frequency of each template, ω_{i_T}, is an approximation of the frequency of the corresponding section:

$$\omega_{i_T} = \frac{\pi}{z_{i+1} - z_i} \tag{12}$$

Then, the template sinusoid $x_{i_T}(n)$ can be expressed as:

$$x_{i_T}(n) = \begin{cases} \pm A_{i_T} sin(\omega_{i_T} n) & \text{if } 0 \le n \le (z_{i+1} - z_i) \\ 0 & \text{if } n > (z_{i+1} - z_i) \end{cases} \tag{13}$$

where $x_{i_T}(n)$ matches the sign of $x_i(n)$. If we split the signal at local extrema to create monotonic segments, the template sinusoid will have the form $A_{i_T} sin(\omega_{i_T} n \pm \frac{\pi}{2})$.

For zero-mean artificial signals, it is usually sufficient to set the template amplitude A_{i_T} to the maximum or minimum value of the current segment. However, for low-SNR signals and multicomponent examples, we choose the A_{i_T} that corresponds to the lowest-cost DTW alignment between the template and the current segment:

$$A_{i_T} = \arg\min_A \{C_{\mathbf{\Omega}} = DTW(x_{i_T}(n), x_i(n))\}, \tag{14}$$

where $C_{\mathbf{\Omega}}$ is the DTW alignment cost defined in (7), and $x_{i_T}(n) = A \cdot sin(\omega_{i_T} n)$.

Because $x_i(n)$ and $x_{i_T}(n)$ are similar, DTW can find a low-cost alignment between these two signals, which can help create a smoother warping path for phase retrieval. Equation (10) requires the inverse of the warping path, which is determined by inverting the axes of the warping path of $DTW(x_{i_T}(n), x_i(n))$.

To further smoothen aberrations in the warping path due to noise, we can elect to fit a polynomial curve to the inverted warping path to obtain an expression for $\mathbf{\Omega}_i^{-1}(k)$. The polynomial fit coefficients are denoted $\left\{\mathbf{\Omega}_{i_0}^{-1}, ..., \mathbf{\Omega}_{i_N}^{-1}\right\}$. The order of the polynomial N is left as a hyperparameter for the algorithm; however, for the examples discussed in this study, N was usually set to 3 or 4.

Assuming the original continuous-time phase $\phi_i(t)$ of the section $x_i(n)$ has the form $\phi_{i_0} + \phi_{i_1} t + ... + \phi_{i_N} t^N$, the sampled phase is $\phi_i(k) = \phi_{i_0} + \phi_{i_1} k T_s + ... + \phi_{i_N} k^N T_s^N$. Using (10),

$$\mathbf{\Omega}_i^{-1}(k) = \frac{1}{\omega_{i_T} T_s}\phi_i(k) = \sum_{j=0}^{N} \frac{\phi_{i_j} k^j T_s^{j-1}}{\omega_{i_T}} \tag{15}$$

Since $\mathbf{\Omega}_i^{-1}(k) = \sum_{j=0}^{N} \mathbf{\Omega}_{i_j}^{-1} k^j$, the predicted phase of the section $x_i(n)$, $\hat{\phi}_i(k)$, is calculated by:

$$\hat{\phi}_i(k) = \sum_{j=0}^{N} \frac{\omega_{i_T}}{T_s^{j-1}} \mathbf{\Omega}_{i_j}^{-1} k^j \tag{16}$$

If polynomial fitting is not desired, the phase estimate can be directly computed from the inverse of the DTW warping path using (5):

$$\hat{\phi}_i(k) = \omega_{i_T} T_s \mathbf{\Omega}_i^{-1}(k) \tag{17}$$

Lastly, the estimates $\hat{\phi}_i(k)$ are concatenated to obtain the entire phase estimate $\hat{\phi}(k)$ for the input signal $x(n)$. To obtain the IF estimate, we compute $\hat{\omega}_i(k) = \frac{1}{2\pi}\frac{\mathrm{d}\hat{\phi}_i(k)}{\mathrm{d}k}$ for each section, and concatenate the results to obtain $\hat{\omega}(k)$. Taking the derivative of each section helps avoid issues of discontinuity at boundary points. The overall approach is summarized in Algorithm 1.

III. Analysis of Artificial Signals

To demonstrate the potentiality of the proposed JADE method, we first consider its performance on three artificial signals and compare it with alternative methods previously proposed in the literature[1].

[1]JADE code and all examples reported in this work are available for download at www.cicone.com

Algorithm 1 JADE($x(n)$, T_s, N).

Inputs: Target signal $x(n)$, sampling period T_s, polynomial fit order N (optional)
Output: Total phase estimate $\hat{\phi}(n)$, IF estimate $\hat{\omega}(n)$

$\mathbf{z} \leftarrow$ Zero-crossings of $x(n)$
$\mathbf{x}_k = \{x_1(n), ..., x_k(n)\} \leftarrow x(n)$ split at crossings $\mathbf{z}$
$\hat{\phi}(n) \leftarrow \{\}$
$k \leftarrow$ length of $\mathbf{z}$
for $i = 1, 2, \ldots, k$ **do**
    $\omega_{i_T} \leftarrow$ template frequency from Eq.(12)
    $A_{i_T} \leftarrow$ template amplitude from Eq.(14)
    $x_{i_T} \leftarrow A_{i_T} sin(\omega_{i_T} n)$
    $\mathbf{\Omega}_i \leftarrow$ warping path of $DTW(x_{i_T}(n), x_i(n))$
    if *polynomial fitting desired* **then**
        Perform N-order polynomial fit to $\mathbf{\Omega}_i^{-1}$
        $\left\{\mathbf{\Omega}_{i_0}^{-1}, ..., \mathbf{\Omega}_{i_N}^{-1}\right\} \leftarrow$ polynomial fit coefficients
        $\hat{\phi}_i(n) \leftarrow$ phase computed from Eq.(16)
    else
        $\hat{\phi}_i(n) \leftarrow$ phase computed from Eq.(17)
    end if
    $\hat{\phi}(n) \leftarrow \left\{\hat{\phi}(n), \hat{\phi}_i(n)\right\}$
end for
return $\hat{\phi}(n), \hat{\omega}(n)$

A. Artificial example 1

The simplest case to consider is the linear chirp signal with quadratic phase and amplitude 1: $x(n) = cos(\alpha n^2 + \beta n) + \gamma\xi_n$, where ξ_n are Gaussian random numbers with zero mean and standard deviation 1, and γ is a scaling factor. In Fig. 2, phase estimation is shown on a quadratic phase signal with γ = 0.05, $\alpha = \frac{\sqrt{2}}{3000}$ and $\beta = \frac{\sqrt{5}}{500}$. The Signal to Noise Ratio (SNR), computed as SNR = $20 \cdot log(\|signal\|_2 / \|noise\|_2)$, of this signal is 23.18 dB. In Fig. 2, we show the result of the JADE phase estimate with and without polynomial fitting, in the bottom and middle panels respectively. In both cases, it can be seen that the phase estimated using JADE matches the ground truth phase function of the signal well.

Different values of SNR were tested to determine the algorithm's resilience to noise. We define the relative error ϵ to be:

$$\epsilon = \frac{\left\|\phi(n) - \hat{\phi}(n)\right\|_2}{\|\phi(n)\|_2}, \tag{18}$$

where the ground truth phase $\phi(n) = \alpha n^2 + \beta n$, and $\hat{\phi}(n)$ is the JADE phase estimate. When testing performance over a range of values of SNR, ground truth zero crossings are used. This ensures that the performance of the JADE algorithm is evaluated independently of zero-crossing detection. The assumption of ground truth zero crossings is close to reality up to considerable levels of noise. Table 1 shows measured values of ϵ for different SNR.

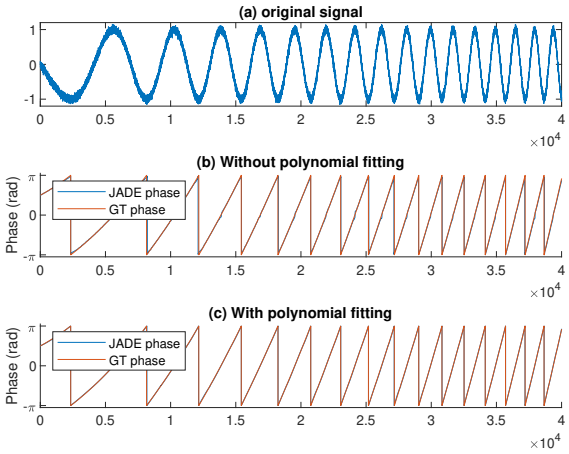

Fig. 2. Phase estimation of a quadratic-phase signal with added Gaussian noise (top). The middle panel shows the JADE-estimated phase (red) and the ground truth (blue) without polynomial fitting. Polynomial fitting can remove slight aberrations in the phase estimate, as seen in the bottom panel.

TABLE I
RELATIVE ERROR IN PHASE ESTIMATE VERSUS NOISE LEVEL

SNR (dB)	ϵ
25.55	0.00015
13.62	0.00055
9.19	0.00089
4.11	0.0012
-1.45	0.0019
-6.36	0.0027
-10.86	0.0040

B. Artificial example 2

The JADE method is next evaluated on a more complicated artificial signal with several components:

$$x(n) = [A(n) \cdot cos(\phi(n))] + \gamma\xi_n, \tag{19}$$

where $A(n) = A_1 cos(\omega_1 n)$, $\phi(n) = n + A_2 cos(\omega_2 n)$, and $\gamma\xi_n$ are Gaussian random numbers with amplitude γ. This signal is amplitude and phase-modulated, as seen in the upper panel of Fig. 3. It is difficult to obtain an expression for the ground truth phase of $x(n)$ from equation 19. To obtain the ground truth phase, we assume that multi-component signals can be considered single-component if the amplitude and frequency components of the signal can be separated. Adapting definition 3.1 from Daubechies et al. [40], we assume the components of a function $f(n) = A(n) \cdot cos(\phi(n))$ can be separated if:

$$|A'(n)|, |\phi''(n)| \leq \epsilon |\phi'(n)|, \forall n \in \mathbb{Z} \tag{20}$$

up to accuracy ϵ. For $x(n)$ in (19), choosing ϵ = 0.01, A_1 = 0.3, ω_1 = 1/35, A_2 = 1, ω_2 = 1/100, and γ = 0.05, the conditions in (20) are satisfied. Therefore for this signal, we assume that the ground truth phase is $\phi(n) = n + cos(n/100)$. In the bottom panel of Fig. 3 the JADE phase estimate is shown in yellow, along with the ground truth phase $\phi(n)$ in red, wrapped to the

range $[-\pi, \pi]$. In this figure, we show the JADE result without using ground-truth zero crossings. We also compare the result to the phase estimate based on the Hilbert Transform (HT). In Fig. 3, the HT phase output is plotted in blue. It can be seen that as the amplitude of the signal decreases, the noise amplitude dominates. In this section, the HT phase estimate becomes erratic, while the JADE phase estimate accurately represents the ground truth phase. The relative error ϵ as defined in (18) between the JADE estimate and the ground truth phase is 0.055.

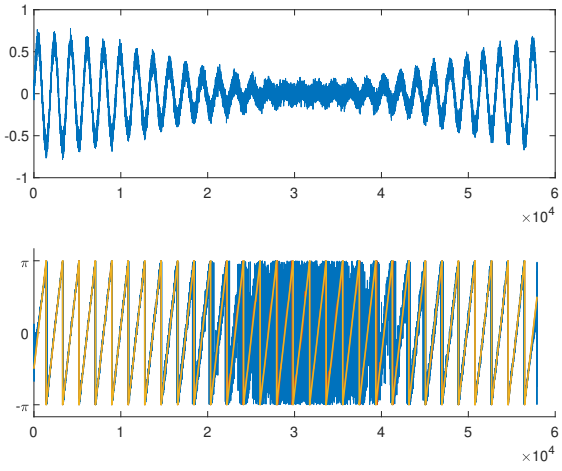

Fig. 3. Original signal from (19) shown in the top panel, with SNR of 28.17 dB. In the bottom panel, the HT phase is shown in blue. The JADE phase estimate (yellow) aligns with the ground truth phase (red).

In Fig. 4, we also show the results of the NHT and DQ methods in estimating the instantaneous phase of the signal in (19) at 28.17 dB SNR. The removal of the AM component causes a visible improvement in the NHT phase compared to the HT phase in Fig. 3. However, both the DQ and NHT phase estimates are erratic in noise. Because the normalization scheme common to both methods involves spline-fitting, the addition of noise can impact this method, and the form of the normalized signal is significantly altered. This can contribute to the inaccuracy in phase estimation seen in Fig. 4.

C. Artificial example 3

As a last example, we consider the solution of the undamped Duffing equation

$$\ddot{x} + \alpha x + \beta x^3 = \gamma \cos(\omega t), \tag{21}$$

which can be rewritten as a spring-mass system with a forcing function

$$\ddot{x} + xk(x) = \gamma \cos(\omega t) \tag{22}$$

where $k(x) = \alpha + \beta x^2$ is a nonlinear spring coefficient which varies with the position x of the mass. Equation (22) can also be interpreted as representing a pendulum with a forcing function and a pendulum length that varies with the angle of the swing. No matter how we interpret physically the equation, (22) solution will be oscillatory with an intrawave modulation

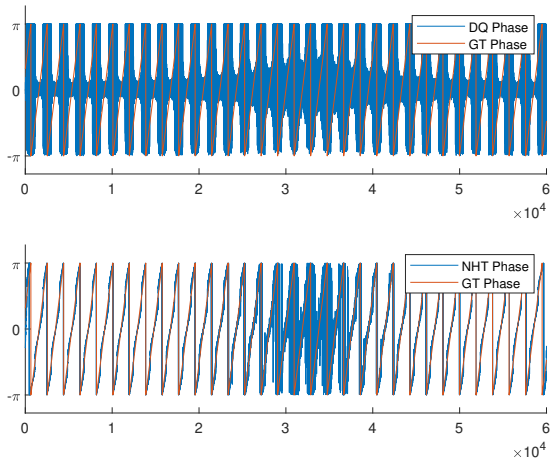

Fig. 4. Outputs of DQ (top) and NHT (bottom) phase estimation algorithms for signal in (19) at 28.17 dB SNR. The ground truth phase is plotted in red in both panels.

in frequency within each period. Continuous changes in the spring constant or length of the pendulum determine constant changes in instantaneous frequency.

If we set $\alpha = -1$, $\beta = 1$, $\gamma = 0.1$, $\omega = 1$, we obtain, through standard numerical integration, the solutions x and $\dot{x}$ plotted in Fig. 5. By considering $\dot{x}$ as the signal we want to analyze, we can decompose it into simple oscillatory components, also called Intrinsic Mode Functions (IMFs) [1]. We can obtain this decomposition, for instance, using the Iterative Filtering algorithm [3]. Each IMF is a mono-frequency signal. The decomposition is shown in Fig. 6.

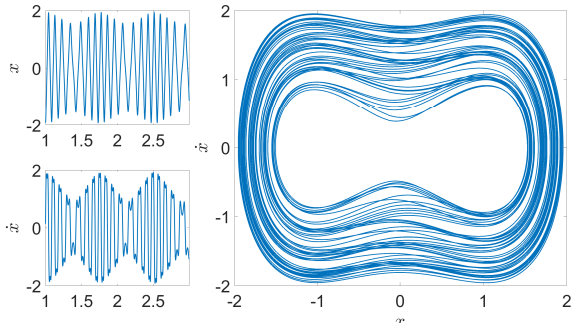

Fig. 5. Solution of the undamped Duffing equation for $\alpha = -1$, $\beta = 1$, $\gamma = 0.1$, and $\omega = 1$.

If we focus our attention on the first 100 seconds of the first IMF extracted from the signal $\dot{x}$, and we apply the Short Time Fourier Transform (STFT), also known as Spectrogram, the Continuous Wavelet Transform (CWT) [41], and the Synchrosqueezing Transform (SST) [40], we obtain the time-frequency plots reported in Fig. 7.

Similarly, on the same signal, we can apply HT [16], IMFogram [33], [34], and the proposed JADE algorithm, ref. Fig. 8.

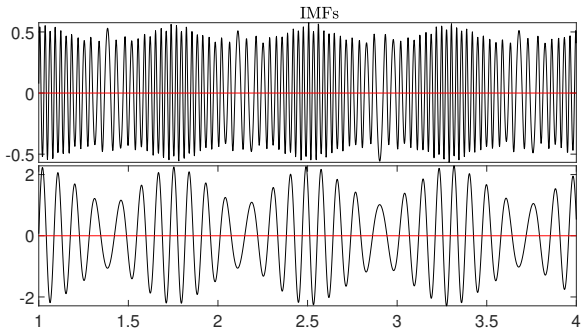

Fig. 6. Iterative Filtering decomposition into mono-frequency signals of $\dot{x}$ solution of the first 4 minutes of the undamped Duffing equation plotted in Fig. 5.

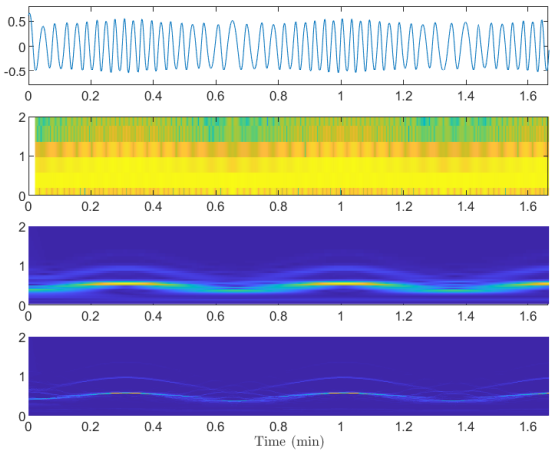

Fig. 7. First IMF of the $\dot{x}$ solution of the undamped Duffing equation (22) (top panel) and IF estimates from STFT (second), CWT (third), and SST (bottom) in Hertz.

From a direct comparison of Fig. 7 and Fig. 8 we can observe that classical methods like STFT, CWT, and the advanced SST have a hard time following the quick local variability in the frequency of this particular signal. These methods, rely on bases whose elements taken individually cannot represent such a signal. This is the reason why we see more than one frequency curve appearing in all time-frequency planes in Fig. 7.

Whereas, using HT, IMFogram, and JADE algorithm we end up having a single frequency curve over time, Fig. 8. These last three methods present similar performance. However, we know from previous tests that among the three, only JADE can produce instantaneous curves, up to numerical precision, and that only JADE is stable to possible noise.

IV. Analysis of Real World Examples

To demonstrate the abilities of the JADE algorithm, we apply it to analyze electrocardiogram (ECG) signals, gravitational wave (GW) signals, and geomagnetic response waveforms.

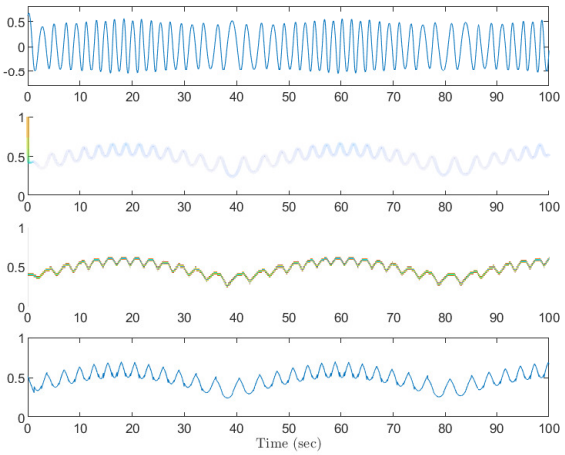

Fig. 8. First IMF of the $\dot{x}$ solution of the undamped Duffing equation (22) (top panel) and IF estimates from HT (second), IMFogram (third), and JADE (bottom) in Hertz.

A. Gravitational Wave Analysis

In this example, we consider the phase estimation of a simulated inspiral gravitational wave (GW) signal. Inspiral GW signals are generated during the end-of-life merging of neutron star or black hole binary systems. There exist many approximate analytical models to simulate inspiral GW waveforms; we use *SEOBNRv4* [42], an effective-one-body (EOB) model employed by the LIGO-VIRGO collaboration. Using the PyCBC software package [43], we simulate an inspiral GW signal using *SEOBNRv4*, with a ringdown time step of 1/8192 and a lower frequency of 40Hz. This simulated waveform is shown in the upper panel of Fig. 9. The ground truth phase and IF are obtained directly from PyCBC. The middle panel shows that the JADE phase estimate matches the ground truth phase, and the bottom panel shows the IF estimate matches the ground truth as well.

Because the ground truth phase and IF are available from the PyCBC module, we test the JADE estimate performance in different noise conditions. We add Gaussian noise to the original waveform to create a range of SNR signals and measure the relative error between the JADE phase estimate and ground truth phase, defined in (18), for each case. The results are summarized in Table 2.

TABLE II
Relative error in phase estimate versus noise level for gravitational waveform

SNR (dB)	ϵ
6.02	0.00072
3.63	0.00055
1.59	0.0011
-1.31	0.0014
-3.41	0.0015
-6.58	0.0018

The -6.58 dB case is shown in Fig. 10. We zoom into the

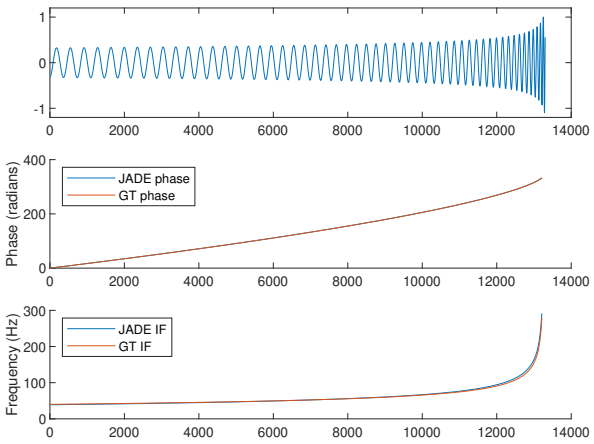

Fig. 9. Simulated inspiral gravitational waveform is shown in the top panel. In the middle panel, the JADE phase estimate (blue) aligns with the ground truth phase from PyCBC (red). Similarly in the bottom panel, the JADE IF (blue) aligns with the ground truth frequency from PyCBC (red).

latter portion of the signal to show the effect of the noise on the gravitational waveform.

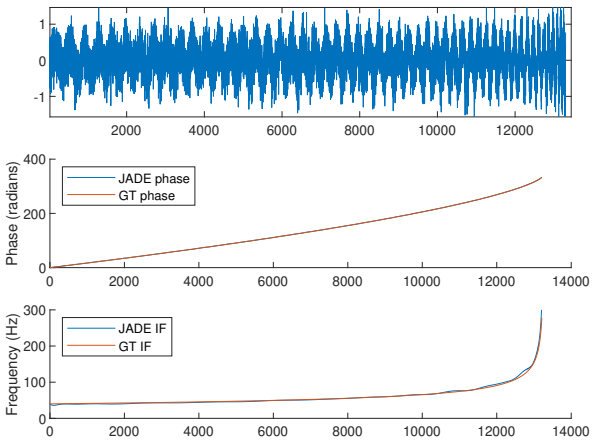

Fig. 10. Simulated inspiral gravitational waveform with added Gaussian noise is shown in the top panel. The phase and IF estimates compared with ground truths are shown in the middle and bottom panels respectively.

B. Electrocardiogram Analysis

We next consider the phase estimation and reconstruction of electrocardiogram (ECG) signals from the MIT-BIH Arrhythmia database publicly available at *PhysioNet* [44]. This database consists of 48 two-channel ECG recordings of approximately 30 minutes in length, from 47 different patients. The recordings were sampled at 360Hz. From a particular recording (serial number 105), we isolate a singular ECG pulse of a duration of 0.7 seconds. We apply a moving average filter in order to remove the high-frequency component from the signal. The resulting signal is shown in the top panel of Fig. 11 in red.

Because the ground truth phase of the ECG signal is unknown, the performance of the JADE phase estimate cannot be directly evaluated. Instead, we perform a reconstruction of the original signal using the JADE phase estimate. We aggregate the sinusoidal template amplitudes into an amplitude function $\hat{A}(n)$, and also construct a function $\hat{\mu}(n)$ that contains the mean values of each section which were removed to perform the phase estimation. Then, to reconstruct the signal from the JADE phase estimate $\hat{\phi}(n)$, we evaluate:

$$\widehat{ECG} = [\hat{A}(n) \cdot cos(\hat{\phi}(n))] + \hat{\mu}(n) \tag{23}$$

The reconstruction $\widehat{ECG}$ is shown in the top panel of Fig. 11 in blue. It can be seen that the reconstruction based on the JADE phase estimate accurately represents the original ECG signal. In the bottom panel, we show the JADE IF estimate along with the HT IF for comparison. However, our approach only provides a singular frequency estimate per time index, while the ECG is clearly a multi-component signal.

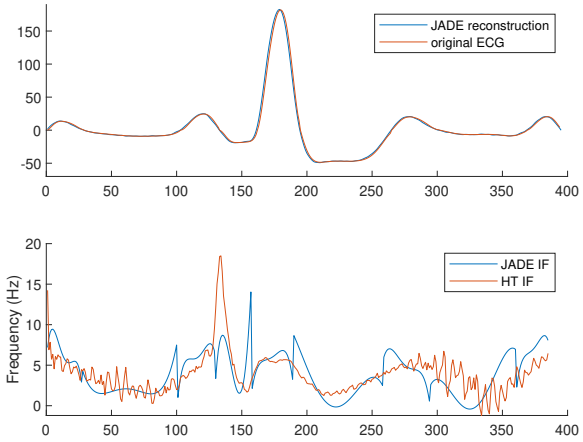

Fig. 11. Top panel shows ECG pulse from MIT-BIH Arrhythmia database (red) and reconstruction of the signal from JADE phase estimate (blue). The bottom panel shows the JADE IF estimate (blue) and HT IF (red).

C. Magnetic Field Response Analysis

In this example, we consider phase estimation of magnetospheric and geomagnetic response to solar wind. Collision of the solar wind with the magnetic field causes a magnetospheric response characterized by sudden enhancement of the magnetic field intensity [45]. We analyze one particular event detected by GEOS (Geostationary Operational Environmental Satellites) spacecraft; this signal is shown in the upper panel of Fig. 12. First, the signal is decomposed into IMFs using the Fast Iterative Filtering (FIF) method. We estimate the phase of the second and third IMFs using JADE and compute the signal reconstruction according to (23) for both IMFs. The results are shown in the middle and bottom panels of Fig. 12.

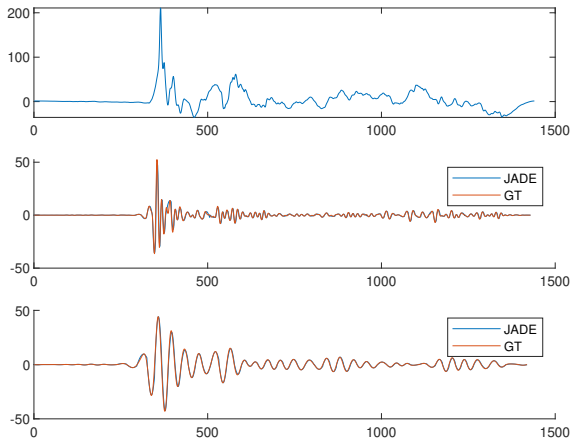

Fig. 12. Top panel shows the original geomagnetic response waveform. The middle and bottom panels show the second and third IMFs respectively (red), and the corresponding reconstructions using JADE phase estimates (blue).

V. Conclusion

Many real-life applications require the analysis of non-stationary signals whose frequencies vary rapidly over time. In recent years many innovative and nonlinear approaches have been proposed for the decomposition of such signals into mono-component signals. Once the signals have been decomposed into mono-component ones, we need to study their phase and frequency content over time with, possibly, high accuracy. In this work, we propose a new approach, called JADE, based on the Dynamic Time Warping method, for the estimation of the instantaneous phase and frequency of a mono-component signal. We test this method on both synthetic and real-life signals comparing results with other algorithms proposed so far in the literature. The results show clearly that JADE outperforms any other method developed so far in the literature and proves to be extremely stable, even in the presence of heavy noise.

Acknowledgment

A. Cicone is a member of the INdAM Research group GNCS and is supported in part by the Italian Ministry of the University and Research under a PRIN PNRR 2022 grant number E53D23018040001.

References

[1] N. E. Huang, Z. Shen, S. R. Long, M. C. Wu, H. H. Shih, Q. Zheng, N.-C. Yen, C. C. Tung, and H. H. Liu, "The empirical mode decomposition and the hilbert spectrum for nonlinear and non-stationary time series analysis," *Proceedings of the Royal Society of London. Series A: mathematical, physical and engineering sciences*, vol. 454, no. 1971, pp. 903–995, 1998.

[2] L. Lin, Y. Wang, and H. Zhou, "Iterative filtering as an alternative algorithm for empirical mode decomposition," *Advances in Adaptive Data Analysis*, vol. 1, no. 04, pp. 543–560, 2009.

[3] A. Cicone and H. Zhou, "Numerical analysis for iterative filtering with new efficient implementations based on fft," *Numerische Mathematik*, vol. 147, pp. 1–28, 2021.

[4] Z. Wu and N. E. Huang, "Ensemble empirical mode decomposition: a noise-assisted data analysis method," *Advances in adaptive data analysis*, vol. 1, no. 01, pp. 1–41, 2009.

[5] T. Y. Hou and Z. Shi, "Adaptive data analysis via sparse time-frequency representation," *Advances in Adaptive Data Analysis*, vol. 3, no. 01n02, pp. 1–28, 2011.

[6] S. Yu, J. Ma, and S. Osher, "Geometric mode decomposition." *Inverse Problems & Imaging*, vol. 12, no. 4, 2018.

[7] K. Dragomiretskiy and D. Zosso, "Variational mode decomposition," *IEEE transactions on signal processing*, vol. 62, no. 3, pp. 531–544, 2013.

[8] J. Gilles, "Empirical wavelet transform," *IEEE transactions on signal processing*, vol. 61, no. 16, pp. 3999–4010, 2013.

[9] G. Barbarino and A. Cicone, "Stabilization and variations to the adaptive local iterative filtering algorithm: The fast resampled iterative filtering method," *arXiv preprint arXiv:2111.02764*, 2021.

[10] B. Boashash, "Estimating and interpreting the instantaneous frequency of a signal. i. fundamentals," *Proceedings of the IEEE*, vol. 80, no. 4, pp. 520–538, 1992.

[11] ——, "Estimating and interpreting the instantaneous frequency of a signal. ii. algorithms and applications," *Proceedings of the IEEE*, vol. 80, no. 4, pp. 540–568, 1992.

[12] L. Cohen, *Time-frequency analysis*. Prentice hall New Jersey, 1995, vol. 778.

[13] P. J. Loughlin and B. Tacer, "Comments on the interpretation of instantaneous frequency," *IEEE Signal Processing Letters*, vol. 4, no. 5, pp. 123–125, 1997.

[14] C. Wang and M. G. Amin, "Performance analysis of instantaneous frequency-based interference excision techniques in spread spectrum communications," *IEEE transactions on Signal Processing*, vol. 46, no. 1, pp. 70–82, 1998.

[15] V. C. Chen and H. Ling, *Time-frequency transforms for radar imaging and signal analysis*. Artech house, 2002.

[16] N. E. Huang, Z. Wu, S. R. Long, K. C. Arnold, X. Chen, and K. Blank, "On instantaneous frequency," *Advances in adaptive data analysis*, vol. 1, no. 02, pp. 177–229, 2009.

[17] H.-t. Wu, "Instantaneous frequency and wave shape functions (i)," *Applied and Computational Harmonic Analysis*, vol. 35, no. 2, pp. 181–199, 2013.

[18] L. Stanković, I. Djurović, S. Stanković, M. Simeunović, S. Djukanović, and M. Daković, "Instantaneous frequency in time–frequency analysis: Enhanced concepts and performance of estimation algorithms," *Digital Signal Processing*, vol. 35, pp. 1–13, 2014.

[19] B. Boashash, *Time-frequency signal analysis and processing: a comprehensive reference*. Academic press, 2015.

[20] H.-T. Wu, "Current state of nonlinear-type time–frequency analysis and applications to high-frequency biomedical signals," *Current Opinion in Systems Biology*, vol. 23, pp. 8–21, 2020.

[21] L. Stankovic, M. Daković, and T. Thayaparan, *Time-frequency signal analysis with applications*. Artech house, 2014.

[22] L. J. Stanković and V. Katkovnik, "Algorithm for the instantaneous frequency estimation using time-frequency distributions with adaptive window width," in *9th European Signal Processing Conference (EUSIPCO 1998)*. IEEE, 1998, pp. 1–4.

[23] I. Djurovic and L. Stankovic, "Modification of the ici rule-based if estimator for high noise environments," *IEEE Transactions on Signal Processing*, vol. 52, no. 9, pp. 2655–2661, 2004.

[24] P. Rao and F. Taylor, "Estimation of instantaneous frequency using the discrete wigner distribution," *Electronics letters*, vol. 4, no. 26, pp. 246–248, 1990.

[25] B. Boashash and P. O'shea, "Use of the cross wigner-ville distribution for estimation of instantaneous frequency," *IEEE Transactions on Signal Processing*, vol. 41, no. 3, pp. 1439–1445, 1993.

[26] P.-L. Shui, H.-Y. Shang, and Y.-B. Zhao, "Instantaneous frequency estimation based on directionally smoothed pseudo-wigner-ville distribution bank," *IET Radar, Sonar & Navigation*, vol. 1, no. 4, pp. 317–325, 2007.

[27] B. Barkat, "Instantaneous frequency estimation of nonlinear frequency-modulated signals in the presence of multiplicative and additive noise," *IEEE Transactions on Signal Processing*, vol. 49, no. 10, pp. 2214–2222, 2001.

[28] I. Djurovic and L. Stankovic, "Robust wigner distribution with application to the instantaneous frequency estimation," *IEEE Transactions on Signal Processing*, vol. 49, no. 12, pp. 2985–2993, 2001.

[29] V. Katkovnik, I. Djurovic, and L. Stankovic, "Instantaneous frequency estimation using robust spectrogram with varying window length," *AEU International Journal of Electronics and Communications*, vol. 54, no. 4, pp. 193–202, 2000.

[30] I. Djurović, M. Urlaub, L. Stanković, and J. F. Böhme, "Estimation of multicomponent signals by using time-frequency representations with application to knock signal analysis," in *2004 12th European Signal Processing Conference*. IEEE, 2004, pp. 1785–1788.

[31] N. A. Khan and B. Boashash, "Instantaneous frequency estimation of multicomponent nonstationary signals using multiview time-frequency distributions based on the adaptive fractional spectrogram," *IEEE Signal Processing Letters*, vol. 20, no. 2, pp. 157–160, 2012.

[32] L. Rankine, M. Mesbah, and B. Boashash, "If estimation for multicomponent signals using image processing techniques in the time–frequency domain," *Signal Processing*, vol. 87, no. 6, pp. 1234–1250, 2007.

[33] P. Barbe, A. Cicone, W. S. Li, and H. Zhou, "Time-frequency representation of nonstationary signals: the imfogram," *Pure and Applied Functional Analysis*, vol. 7, no. 1, pp. 27–39, 2022.

[34] A. Cicone, W. S. Li, and H. Zhou, "New theoretical insights in the decomposition and time-frequency representation of nonstationary signals: the imfogram algorithm," *preprint*, 2023. [Online]. Available: https://arxiv.org/pdf/2205.15702.pdf

[35] R. J. Martis, U. R. Acharya, and H. Adeli, "Current methods in electrocardiogram characterization," *Computers in biology and medicine*, vol. 48, pp. 133–149, 2014.

[36] M. C. Miller and N. Yunes, "The new frontier of gravitational waves," *Nature*, vol. 568, no. 7753, pp. 469–476, 2019.

[37] T. Loto'aniu, R. Redmon, S. Califf, H. Singer, W. Rowland, S. Macintyre, C. Chastain, R. Dence, R. Bailey, E. Shoemaker *et al.*, "The goes-16 spacecraft science magnetometer," *Space Science Reviews*, vol. 215, pp. 1–28, 2019.

[38] E. Bedrosian and A. Nuttall, "On the quadrature approximation to the hilbert transform of modulated signals," *Proc. IEEE*, vol. 51, pp. 868–869, 1963.

[39] A. Nuttall and E. Bedrosian, "On the quadrature approximation to the hilbert transform of modulated signals," *Proceedings of the IEEE*, vol. 54, no. 10, pp. 1458–1459, 1966.

[40] I. Daubechies, J. Lu, and H.-T. Wu, "Synchrosqueezed wavelet transforms: An empirical mode decomposition-like tool," *Applied and Computational Harmonic Analysis*, vol. 30, no. 2, pp. 243–261, 2011.

[41] P. Flandrin, *Time-frequency/time-scale analysis*. Academic press, 1998.

[42] A. Bohé, L. Shao, A. Taracchini, A. Buonanno, S. Babak, I. W. Harry, I. Hinder, S. Ossokine, M. Pürrer, V. Raymond, T. Chu, H. Fong, P. Kumar, H. P. Pfeiffer, M. Boyle, D. A. Hemberger, L. E. Kidder, G. Lovelace, M. A. Scheel, and B. Szilágyi, "Improved effective-one-body model of spinning, nonprecessing binary black holes for the era of gravitational-wave astrophysics with advanced detectors," *Physical Review D*, vol. 95, no. 4, Feb. 2017.

[43] A. Nitz, I. Harry, D. Brown, C. M. Biwer, J. Willis, T. D. Canton, C. Capano, T. Dent, L. Pekowsky, G. S. C. Davies, S. De, M. Cabero, S. Wu, A. R. Williamson, D. Macleod, B. Machenschalk, F. Pannarale, P. Kumar, S. Reyes, Dfinstad, S. Kumar, M. Tápai, L. Singer, P. Kumar, B. U. V. Gadre, Maxtrevor, Veronica-Villa, S. Khan, S. Fairhurst, and K. Chandra, "gwastro/pycbc: v2.3.2 release of pycbc," nov 2023.

[44] G. B. Moody and R. G. Mark, "Mit-bih arrhythmia database," 1992. [Online]. Available: https://physionet.org/content/mitdb/

[45] M. Piersanti and U. Villante, "On the discrimination between magnetospheric and ionospheric contributions on the ground manifestation of sudden impulses," *Journal of Geophysical Research: Space Physics*, vol. 121, no. 7, pp. 6674–6691, 2016.